Electronic Supplementary Material (ESI) for Journal of Materials Chemistry A.

Unidirectional, Highly Linear Strain Sensors with Thickness-Engineered Conductive Films for Precision Control of Soft Machines

Saeb Mousavi, Mai Thanh Thai, Morteza Amjadi, David Howard, Shuhua Peng, Thanh Nho Do, Chun H. Wang

Supporting Information

Contents:

Effect of pre-stretching
Infill analysis
Figures S1-S7
Movie S1
Table S1

Effect of pre-stretching

An important factor that contributed to enhancing the sensors' performance is the pre-stretch level. Pre-stretching is a technique used in crack-based strain sensors for improving sensitivity and linearity [33]. The sensors exhibited enhanced sensitivity and linear strain range after pre-stretching at a higher strain. The results in Figures S1(C-E) show that when PEDOT, PEDOT-CNF and High-conc. PEDOT-CNF sensors were pre-stretched to 50%, 100% and 150% strain, respectively, their gauge factors were increased by 228% (from 127 to 417), 89% (from 147 to 278) and 71% (from 87 to 149), respectively. A comparison of the hysteresis behavior for as-made and pre-stretched sensors is presented in Figures S1C and D, indicating that without pre-stretching, the sensors have a wider hysteresis loop than after being pre-stretched. In addition, the pre-stretched sensor showed a much more stable response during the first 10 cycles with a significantly better linear working range.

Infill analysis

The actual printing density is calculated using the equation given in [31] and it is different from the nominal infill% set in the printer software (Simplify3D). The actual infill% values were calculated from the optical images shown in Figure S5. For infill densities greater than 90%, the printed tracks tend to randomly connect at different locations. In this case, we calculated the average infill density by measuring the infill density for all pairs of printed tracks in the image.

infill% $= \frac{b}{a}$ ("b" and "a" are shown in Figure S5(D))

80% nominal ➔ actual infill% = $\frac{b}{a} \times 100 = 56.6\%$

90% nominal ➔ actual infill% = $\frac{avg(b)}{avg\ (a)} \times 100 = 72.8\%$

100% nominal ➔ actual infill% = $\frac{avg(b)}{avg\ (a)} \times 100 = 97.2\%$

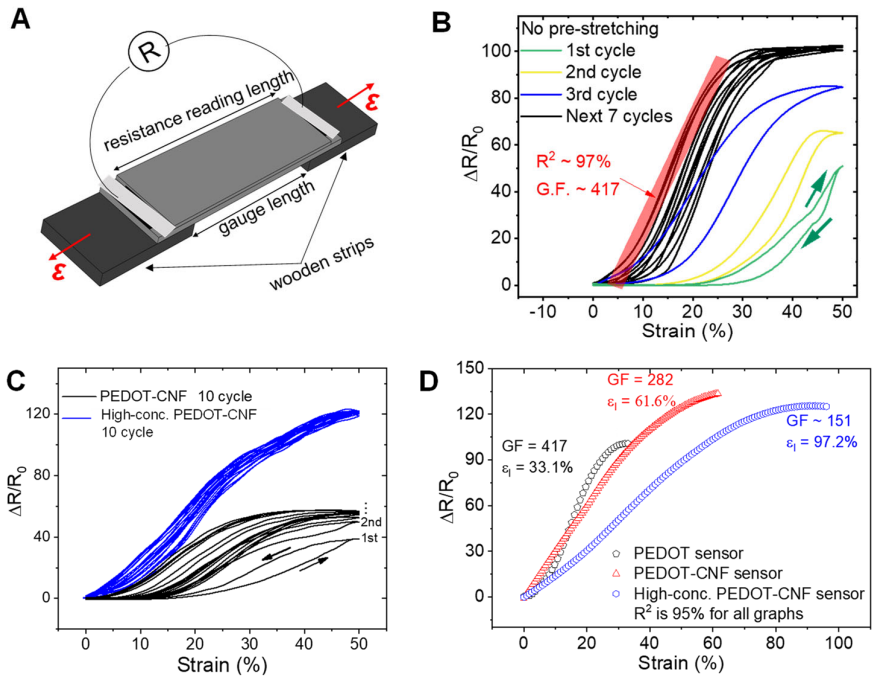

Figure S1. (**A**) The sensors were glued at the back on two wooden strips for tensile tests and the resistance is measured from outside the glued spots. (**B**) The resistance changes of the 3D printed PEDOT sensor in the strain domain for the first ten cycles of repeated stretching at 50% strain showing the effect of pre-stretching. (**C**) The resistance changes of the 3D printed PEDOT:PSS-CNF sensor for the first ten cycles of repeated stretching at 50% strain (black curves), and the resistance changes of the 3D printed PEDOT:PSS-CNF sensor for the ten cycles of repeated 50% stretching after being pre-stretched to 100% strain (blue). (**D**) The linear operation range of PEDOT sensor (ε_I ~ 33%), PEDOT:PSS-CNF sensor (ε_I ~ 61%), and high-conc. PEDOT:PSS-CNF sensors (ε_I ~ 97%) are shown in black, red, and blue, respectively.

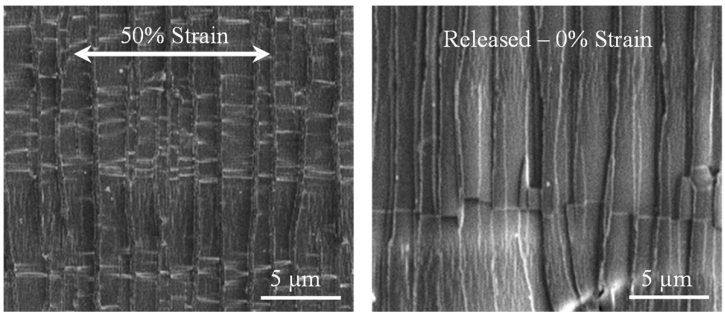

Figure S2. The Region *ii* of the PEDOT sensor under 50% strain and after strain release. Once the strain was released, the generated crack edges were re-connected.

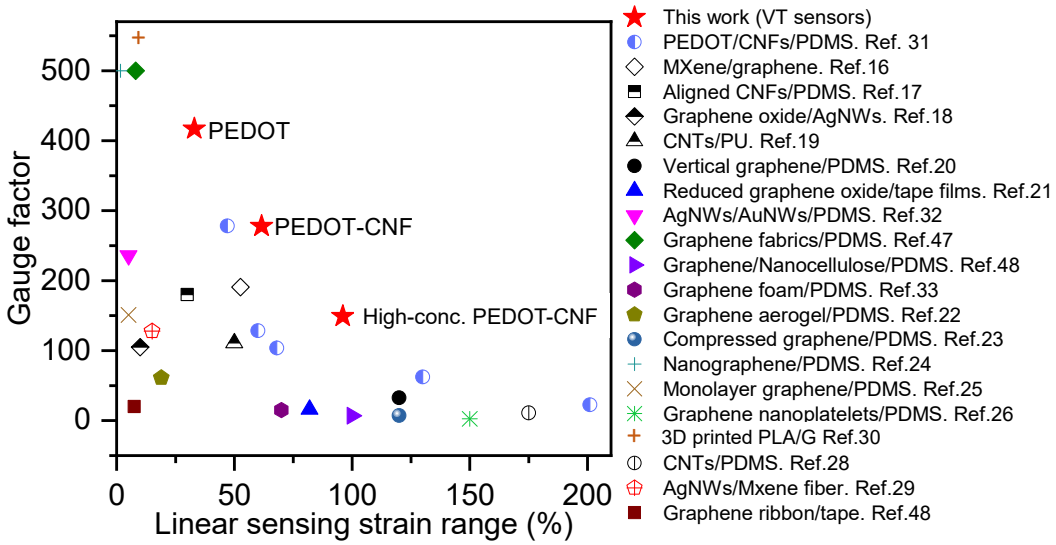

Figure S3. Comparison of sensing performance in terms of GF and linear sensing range of strain sensors in this work (PEDOT, PEDOT-CNF, and high-conc. PEDOT-CNF sensors) with the recently reported ones in the literature. The current sensors show superior performance compared to the previously reported sensors.

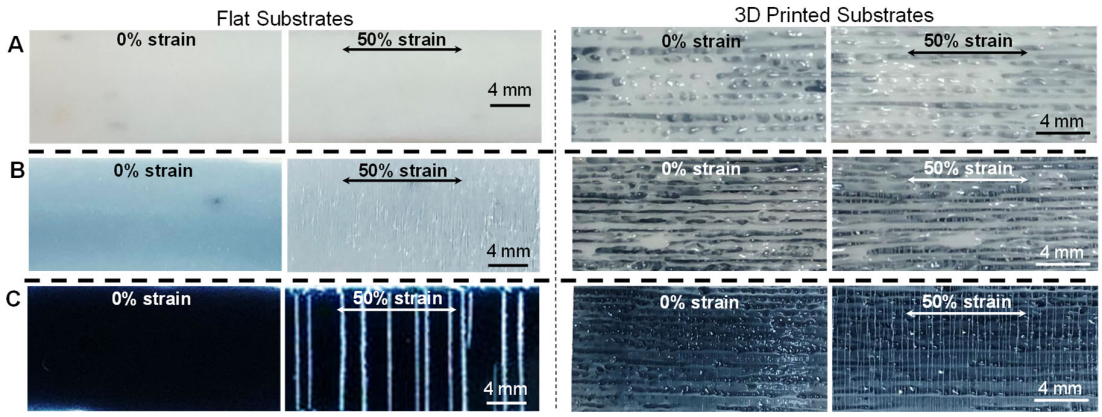

Figure S4. Crack morphology comparison between PEDOT sensors coated on flat and 3D printed substrates. (**A-C**) Optical images of the PEDOT sensors with a thickness of 42, 324, and 655 nm, respectively at rest (0% strain) and under 50% strain.

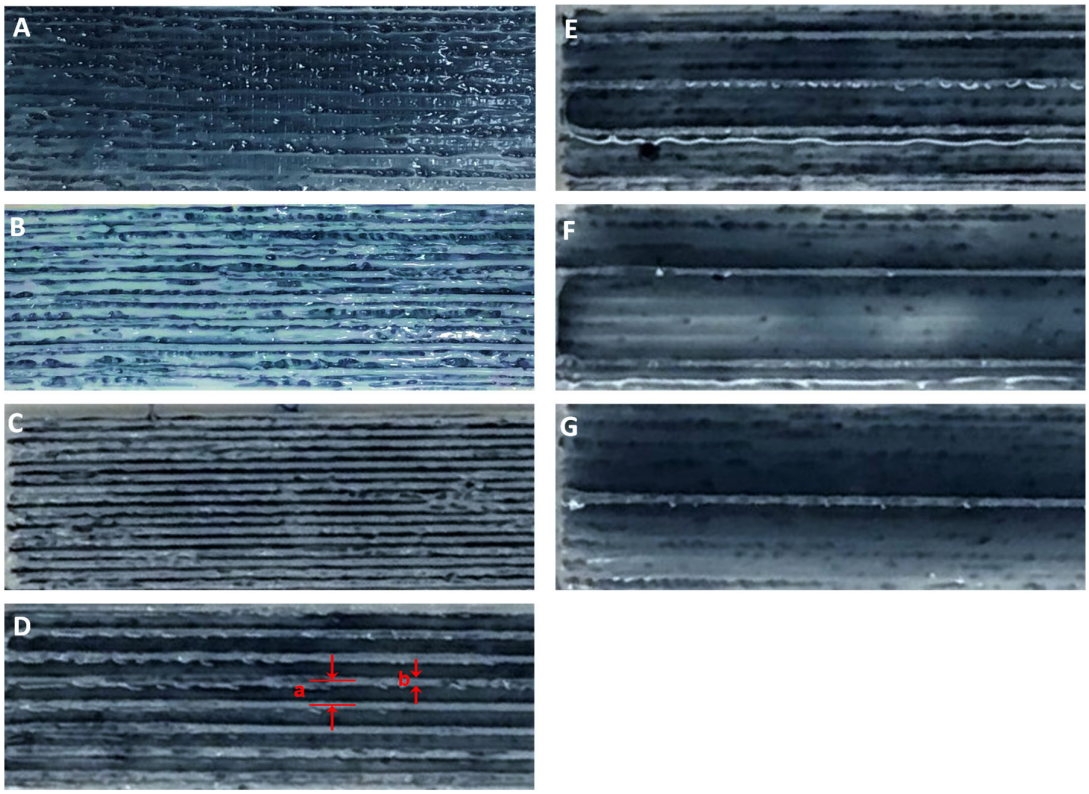

Figure S5. Top-view optical images of the PEDOT sensors coated on 3D printed TPU substrates with different infill densities: (**A**) 100%, (**B**) 90%, (**C**) 80%, (**D**) 40%, (**E**) 20%, (**F**) 10%, (**G**) 5%.

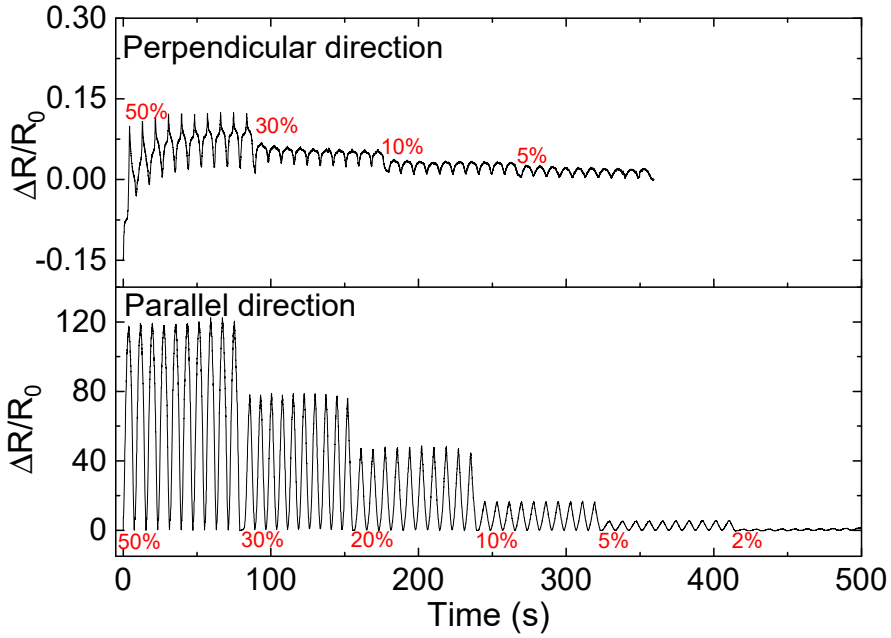

Figure S6. The resistance change of the VT sensor when stretched in parallel and perpendicular to the printing directions.

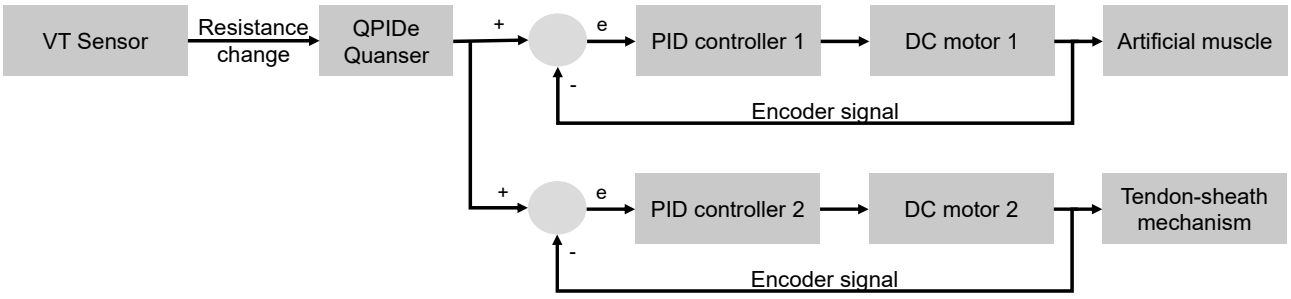

Figure S7. The control flow of the robotic catheter. The actuation commands in two DC motors are regulated by two simple PID controllers for the movement of each element of the robotic catheter, the gripper (tendon-sheath mechanism), and the tentacle (artificial muscle).

Movie S1. Demonstration of catheter control with our VT sensors

Table S1. 3D printing parameters for printing the TPU structure

Parameter	**Structural Material** TPU Ninjaflex (clear)
Filament Diameter (mm)	1.75
Nozzle Diameter (mm)	0.4
Nozzle Temperature (°C)	230
Bed Temperature(°C)	40
Printing Speed (mm/s)	500
Nominal Infill Density (%)	Variable for sensor substrate layer 100% for all other layers
Bottom Solid Layers (#)	1
Top Solid Layers (#)	0
Layer Height (mm)	0.2
Number of Shells	1
Track Width (mm)	450
Cooling Fan (%)	0
Support	None
Infill Pattern	Rectilinear
Raster Angle (°) (Print Direction)	0, 90 (alternating)